6th AIAA Theoretical Fluid Mechanics Conference
27 - 30 June 2011, Honolulu, Hawaii

AIAA 2011-3603

Check for updates

Towards the foundation of a global modes concept

Daniel Rodríguez[†*], Anatoli Tumin[‡] and Vassilis Theofilis[*]

[†] *California Institute of Technology, Pasadena, CA 91125, USA*

[‡] *The University of Arizona, Tucson, AZ 85721, USA*

[*] *School of Aeronautics, Universidad Politécnica de Madrid,*
Pza. Cardenal Cisneros 3, E-28040 Madrid, SPAIN

A contribution is presented, intended to provide theoretical foundations for the ongoing efforts to employ global instability theory for the analysis of the classic boundary-layer flow, and address the associated issue of appropriate inflow/outflow boundary conditions to close the PDE-based global eigenvalue problem in open flows. Starting from a theoretically clean and numerically simple application, in which results are also known analytically and thus serve as a guidance for the assessment of the performance of the numerical methods employed herein, a sequence of issues is systematically built into the target application, until we arrive at one representative of open systems whose instability is presently addressed by global linear theory applied to open flows, the latter application being neither tractable theoretically nor straightforward to solve by numerical means.

Experience gained along the way is documented. It regards quantification of the departure of the numerical solution from the analytical one in the simple problem, the generation of numerical boundary layers at artificially truncated boundaries, no matter how far the latter are placed from the region of highest flow gradients and, ultimately the impractically large number of (direct and adjoint) modes necessary to project an arbitrary initial perturbation and follow its temporal evolution by a global analysis approach, a finding which may question the purported robustness reported in the literature of the recovery of optimal perturbations as part of global analyses yielding under-resolved eigenspectra.

Downloaded by Anatoli Tumin on August 27, 2019 | http://arc.aiaa.org | DOI: 10.2514/6.2011-3603

I. Introduction

Global stability analysis via the solution of two-dimensional partial-derivative-based eigenvalue problems, and the use of global modes in the study of a variety of complex (and "simple") flow configurations have experienced recent progress in the last decade, impulsed by the advances in the algorithmic methods and computational capabilities. The global stability approach has thus become a common practice in the study of flow perturbations and theoretical flow control applications[1–8] A recent review on the work done in this field may be found in Ref. 9.

While many efforts have been spent, aiming at applying global modes to the solution of physical problems, the mathematical foundations of the global mode representation have not received the same degree of attention, if not completely left aside. Global modes have been shown to be physically insightful and theoretically founded in the case of the so-called "oscillator"-type instability, in which a single global eigenmode corresponds with a physical instability mode. This is the only kind of instability possible in closed flows, where the limits of the computational domain (or the "box") are unequivocally defined, as are the boundary conditions to be imposed. Oscillator-type instability can also exist in open flows, but the origin of the instability is highly localized in space and the eigenmode representing the instability is robust against changes in the "box" and the boundary conditions, provided that the box is big enough.[10] The main concerns are related to the application of a global mode approach to convective instabilities (or so-called "amplifiers"). In this case the flow is globally stable (perturbations will decay if unforced) but external excitations are spatially amplified. The description of convective instabilities in terms of global modes requires a projection onto the normal modes of the open flow.

The formulation of global eigenvalue problems in open flows is accompanied by some uncertainties in the "box" truncation and the choice of boundary conditions over a 2D domain. The choice of boundary conditions

Copyright © 2011 by Daniel Rodriguez. Published by the American Institute of Aeronautics and Astronautics, Inc., with permission.

has a heuristic nature, and this provokes questions regarding the suitable formulation of the eigenvalue problems. Most of the work done on amplifier-type instability considered boundary layer flows, either on a simple zero-pressure-gradient flat plate or in a flat plate with mild geometrical protrusions or shallow cavities. The analysis of the weakly non-parallel Blasius flow can be addressed using the classic Orr-Sommerfeld equation, and has also been carried out in a global "box formulation" in Refs. 2, 3. A comprehensive analysis of the upstream and downstream boundary conditions' effect on the spectrum of parallel boundary-layer flow was carried out in Ref. 4. These explorations shed some light onto the representation of discrete Tollmien-Schlichting modes within the "box formulation." However, because the underlying complexity of the 2D eigenvalue problem demands significant computational power, there is still a lack of understanding of the qualitative features of this advanced formulation.

In this paper, a simple model is presented that can help to understand the effect of the upstream and downstream boundary conditions on the eigenvalues and eigenfunctions of open flows, and possible limitations of the global formulation. A uniform unbounded incompressible flow is considered, for which a normal mode decomposition can be done in terms of a continuous spectrum of vorticity modes. In order to understand the effect of domain truncation and boundary conditions in the "box formulation", an intermediate formulation is introduced that considers a "tall box", unbounded in the transversal direction. The "tall box" formulation sheds light on some characteristics of the global modes, the origin of which was erroneously attributed to physical reasons in the literature. Finally, the solution of the initial value problem based on a normal mode projection is considered, showing possible limitations of the global formulation in dealing with convective instabilities and theoretical flow control of open flows.

Downloaded by Anatoli Tumin on August 27, 2019 | http://arc.aiaa.org | DOI: 10.2514/6.2011-3603

II. A model problem: uniform flow

To make the model as transparent as possible, the initial-value problem in a uniform incompressible flow ($U_\infty = const$) is considered here. The solution of this problem can be found analytically using the Laplace transform in time and Fourier transform in x- and y- directions. There are no discrete normal modes, and the solution can be presented as an expansion into the vorticity modes of the continuous spectrum. For a given streamwise wave number, α, and transversal wave number, k, the vorticity modes have complex frequency $\omega = \alpha - i\left(k^2+\alpha^2\right)/R$, where R is the Reynolds number based on the free stream velocity, U_∞, and on the appropriate length scale L. Let's address the known problem using the "box formulation" for a 2D domain: $x = [-L_x, L_x], y = [-L_y, L_y]$. It is still a challenging problem if we use advanced computational tools to shed some qualitative light onto the effect of the boundary conditions on the 2D normal modes. In order to elucidate the features of using the "box formulation", let's consider a case when $L_y \gg L_x$. In the limit of the "tall" box, we arrive at a consideration of the strip $x = [-1, 1], y = (-\infty, +\infty)$ (L_x is the length scale). The limit allows Fourier transform in y similarly to analysis in,[11] in which the strip of uniform flow with inhomogeneous upstream and downstream boundary conditions for perturbations was considered. Here, we use the same model of perturbations in a strip of uniform flow, but we formulate homogeneous boundary conditions at $x = -1$, and $x = +1$.

The linearized Navier-Stokes equations can be written in the matrix-vector form:

$$ik\mathbf{A} - i\omega\mathbf{H}_t\mathbf{A} = \mathbf{H}_1\mathbf{A} + \mathbf{H}_2\frac{d\mathbf{A}}{dx}, \tag{1}$$

where $\mathbf{H}_t, \mathbf{H}_1$, and $\mathbf{H}_2$ are 4×4 matrices. Vector $\mathbf{A} = (u, p, v, \Omega)^T$ is comprised of the pressure perturbation p, x- and y- velocity components u and v, respectively; $\Omega = \partial u/\partial y - \partial v/\partial x$. The solution of the system of ODEs with constant coefficients can be written in the form: $\mathbf{A} = \sum_{j=1}^{4} C_j\mathbf{Z}_j \exp(\lambda_j x)$, where

$$\lambda_1 = -k, \lambda_2 = k, \lambda_3 = \frac{1}{2}\left(R - \sqrt{4k^2+R^2-4iR\omega}\right), \lambda_4 = \frac{1}{2}\left(R + \sqrt{4k^2+R^2-4iR\omega}\right), \tag{2}$$

$$\begin{gathered}
\mathbf{Z}_1 = \left(i, -i\tfrac{k+i\omega}{k}, 1, 0\right)^T, \mathbf{Z}_2 = \left(-i, i\tfrac{k-i\omega}{k}, 1, 0\right)^T, \\
\mathbf{Z}_3 = \left(\tfrac{2ik}{-R+\sqrt{4k^2+R^2-4iR\omega}}, 0, 1, \tfrac{R\left(R-2i\omega-\sqrt{4k^2+R^2-4iR\omega}\right)}{-R+\sqrt{4k^2+R^2-4iR\omega}}\right)^T, \\
\mathbf{Z}_4 = \left(-\tfrac{2ik}{R+\sqrt{4k^2+R^2-4iR\omega}}, 0, 1, -\tfrac{R\left(R-2i\omega+\sqrt{4k^2+R^2-4iR\omega}\right)}{R+\sqrt{4k^2+R^2-4iR\omega}}\right)^T.
\end{gathered} \tag{3}$$

The first and the second fundamental solutions can be interpreted as "pressure waves" (they have zero vorticity and non-zero pressure). The third and the fourth fundamental solutions can be interpreted as "vorticity waves" (they have zero pressure and non-zero vorticity). The coefficients C_j are determined from the boundary conditions. The box formulation delivers the pressure perturbation. The downstream and upstream pressure waves are localized within the layers having an order of magnitude $\sim 1/|k|$. In order to have a reasonable approximation of the unbounded domain, one has to consider perturbations having the characteristic scale $l_y \ll 1$, and to keep in mind that the solution is affected by the boundary conditions within the layers $x \approx [-1, -1 + l_y]$ and $x \approx [1 - l_y, 1]$. At finite k and $R \gg 1$, one can find:

$$\lambda_3 \approx i\omega - \frac{k^2 + \omega^2}{R}, \quad \lambda_4 \approx R - i\omega.$$

The third fundamental solution represents a vorticity mode propagating with the flow and slowly decaying due to the viscosity. The forth fundamental solution represents a vorticity perturbation stemming from the right boundary ($x = 1$) and localized within the layer of thickness $O(1/R)$.

II.A. Tall-box formulation with homogeneous Dirichlet boundary conditions

Consider an example of the boundary conditions:

$$u(-1) = v(-1) = 0; \quad u(1) = v(1) = 0.$$

Homogeneous boundary conditions lead to a dispersion relation $\omega = \omega(R, k)$. The dispersion relation can be written in the form:

$$\begin{aligned} \Delta(k, R, \omega) = -2k\sqrt{4k^2 + R^2 - 4iR\omega}\,\mathrm{Cosh}(R) + \\ k\sqrt{4k^2 + R^2 - 4iR\omega}\,\mathrm{Cosh}\left(2k - \sqrt{4k^2 + R^2 - 4iR\omega}\right) + \\ k\sqrt{4k^2 + R^2 - 4iR\omega}\,\mathrm{Cosh}\left(2k + \sqrt{4k^2 + R^2 - 4iR\omega}\right) + \\ 2\left(-2k^2 + iR\omega\right)\mathrm{Sinh}(2k)\,\mathrm{Sinh}\left(\sqrt{4k^2 + R^2 - 4iR\omega}\right) = 0 \end{aligned} \tag{4}$$

The eigenvalues can be found as roots of $\Delta(k, R, \omega) = 0$. One can also approach the problem directly by using the spectral collocation method (SCM) for the system of ODEs. In this case Chebyshev polynomials are used to discretize the x direction. In the numerical implementation of the spectral collocation method, nth order Chebyshev polynomials were used with the collocation points

$$\xi = \cos(\pi j/n), \qquad j = 0, ..., n. \tag{5}$$

The discretization of the equations leads to a generalized eigenvalue problem that was solved using two different solvers. The first one utilized an IMSL routine. The other solver used a matrix inversion leading to a standard eigenvalue problem that was solved using a LAPACK routine. Results obtained using these two solvers were in good agreement. Figure 1 shows the convergence test at $R = 1000$ and $k = 2$ depending on the order of the Chebyshev polynomials, n. Most of the following computations were carried out at $n = 150$.

Figure 2 illustrates the spectrum when parameter k is varied (obtained using Mathematica) and results obtained using SCM at $k = 2$ and 5, $R = 100$ and $R = 1000$. It is worth mentioning that the lines in Figure 2 are skewed at their tips similarly to global spectra [Fig. 14,15 and see e.g. Fig. 2 in Ref. 3]. In the unbounded domain, the continuous spectrum represented by the vorticity modes corresponds to a straight line in the complex plane ω. In the case of the tall box formulation, the tips of the modes correspond to small k, and they are affected by the boundary conditions. In the case of the bounded domain, the lines corresponding to the continuous spectrum have been discretized according to the domain extension, number of discretization points and choice of boundary conditions.

Comparisons of the streamwise velocity perturbation obtained using Mathematica and the SCM at $R = 100$ and $R = 1000$ are shown in Fig. 3a and 3b, respectively. Visually, the velocity profiles are very close at both Reynolds numbers. Figure 4a shows the streamwise velocity profiles on the same plot. One can see that they are almost identical. The main difference between the profiles occurs in the boundary layers having thickness $O(R^{-1})$ in the vicinity of $x = 1$ (Fig. 4b).

Figure 5 shows the real and imaginary parts of modes 1 through 4 at $R = 1000$ and $k = 5$. One can see that all the streamwise velocity amplitude in all these modes increases toward the end of the interval. It is

Downloaded by Anatoli Tumin on August 27, 2019 | http://arc.aiaa.org | DOI: 10.2514/6.2011-3603

Downloaded by Anatoli Tumin on August 27, 2019 | http://arc.aiaa.org | DOI: 10.2514/6.2011-3603

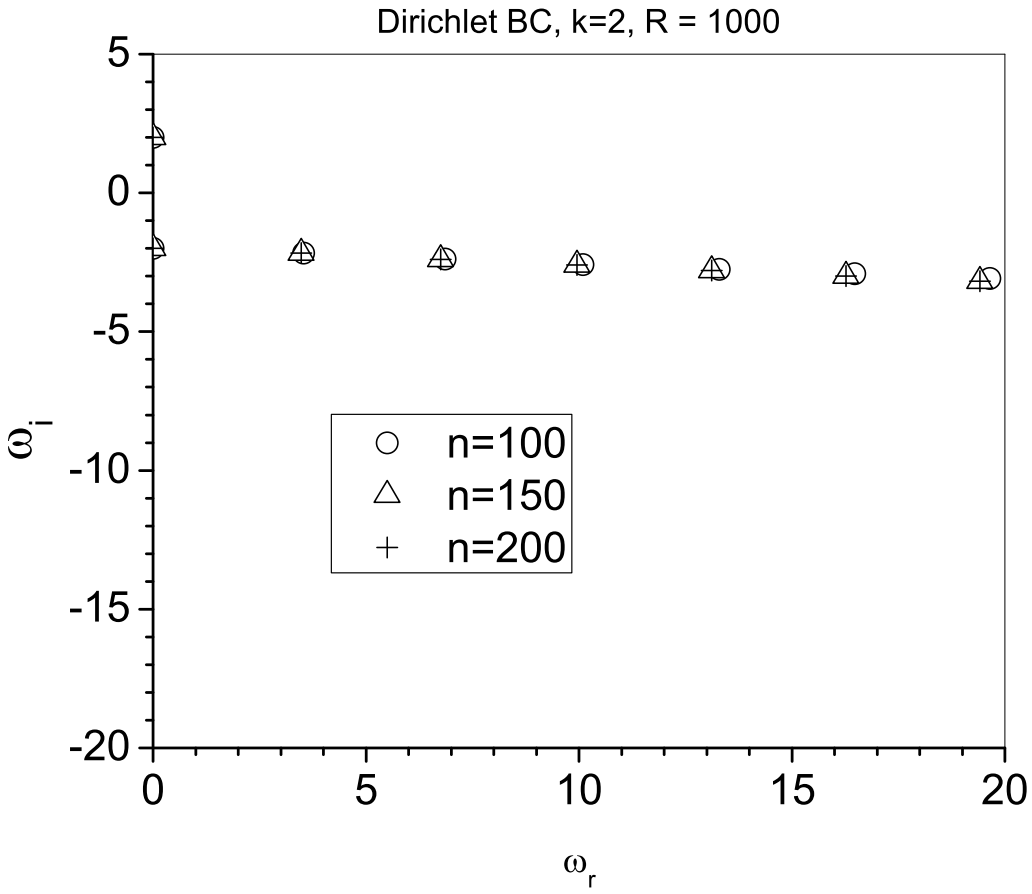

Figure 1. Convergence test at $R = 1000$.

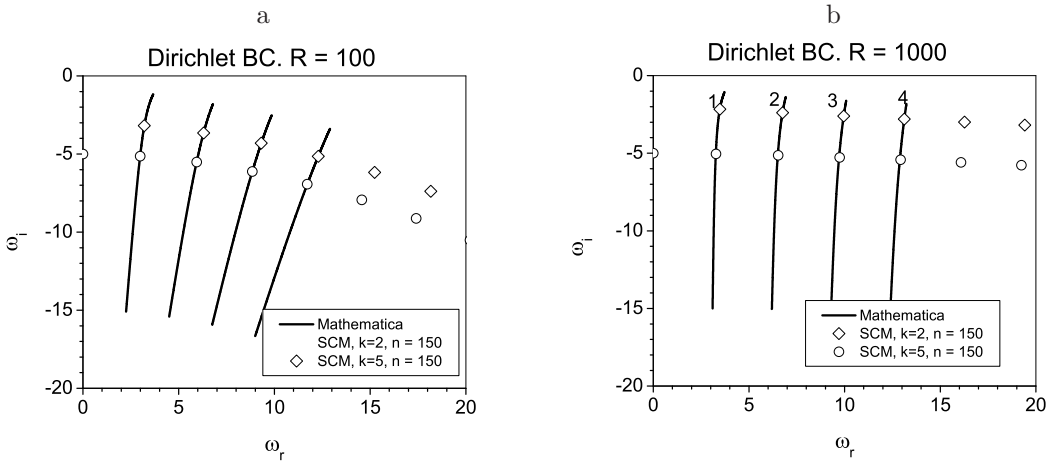

Figure 2. Comparison of SCM results with results obtained using Mathematica for spectrum at $R = 100$ (a) and $R = 1000$ (b), respectively.

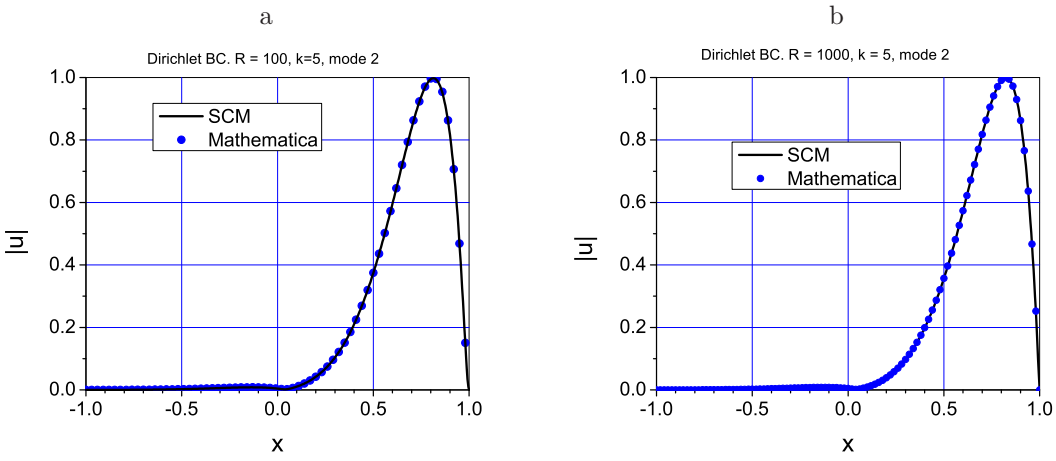

Figure 3. Comparison of SCM results with results obtained using Mathematica for the streamwise velocity perturbation at $R = 100$ (a) and $R = 1000$ (b), respectively.

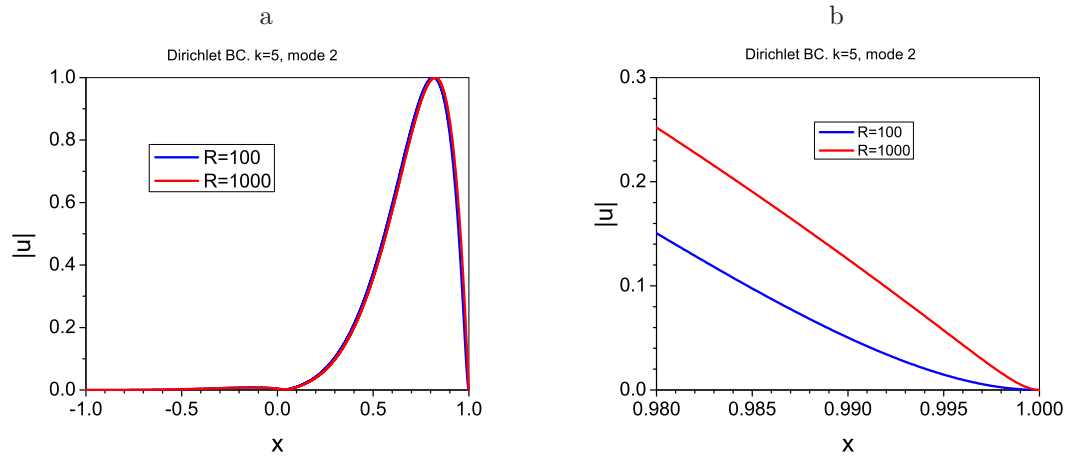

Figure 4. Comparison of the streamwise velocity profiles at $R = 100$ (a) and $R = 1000$ (b), respectively.

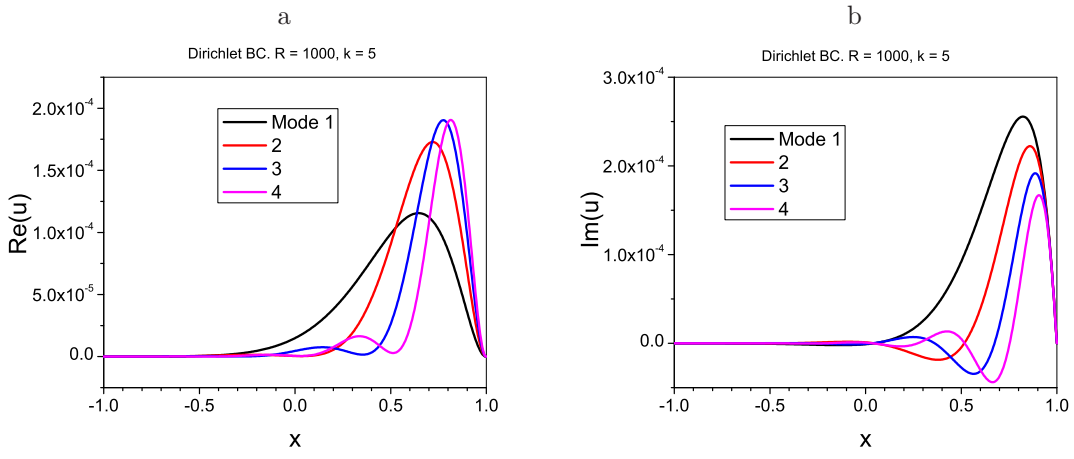

Figure 5. Real and imaginary parts of the streamwise velocity in modes 1 through 4 at $R = 1000$ and $k = 5$.

Downloaded by Anatoli Tumin on August 27, 2019 | http://arc.aiaa.org | DOI: 10.2514/6.2011-3603

tempting to say that the temporal global modes also reflect the spatial amplification, but such a statement apparently is irrelevant to the physical problem, and is a pure effect of the downstream boundary condition.

The boundary layer at the vicinity of $x = 1$ certainly may create a challenge for computing of spectrum and eigenfunctions. The boundary layer for the vertical velocity perturbation, v, is illustrated in Fig. 6. One can see a drastic change in the velocity profile within the layer of $O(R^{-1})$.

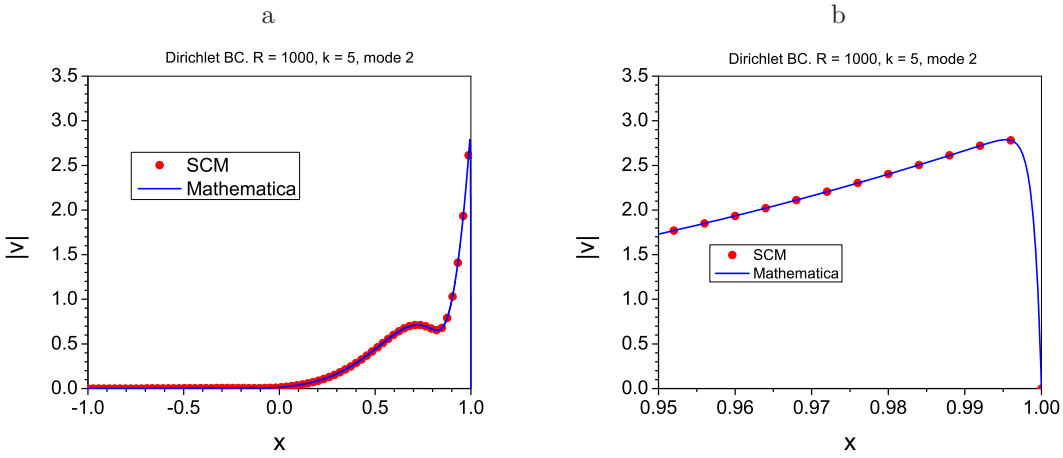

Figure 6. Comparison of SCM results with results obtained using Mathematica for the vertical velocity perturbation at $R = 1000$ and $k = 5$.

If the boundary layer is not resolved accurately, it can cause an error in computation of the spectrum. Figures 7 and 8 illustrate spectrum at $R = 1000$, $k = 5$, $L_x = 1$, and $L_x = 2$ using the grid

$$x = \frac{a(1+\xi)}{(b+\xi)} - L_x,$$
$$b = \frac{L_x}{x_i}, \qquad a = L_x(b+1). \tag{6}$$

where ξ is defined in Eq. (5) and $x_i = 0.5$. Parameter $0 < x_i < 1$ determines the interval $[x_i, L_x]$ where 50% of the grid points are located. One can see (Fig. 8) that increase of the box width leads to a shift in the spectrum similarly observation in Ref. [2]. However, the spectrum shift is an artifact because stretching of the box width led to a lower resolution of the boundary layer. Figure 9 illustrates distribution of the grid points at $x_i = 0.5$ (grid 1) and $x_i = 0.9$ (grid 2). Comparison of the spectrum at $L_x = 1$ (grid 1) and $L_x = 2$ (grid 2) is shown in Fig. 10. One can see that there is no shift of the spectrum . One can notice splitting of the spectrum at large ω_r and $L_x = 2$. The spectrum splitting is similar to observation in Fig. 2 of Ref.[3] for mode m_1.

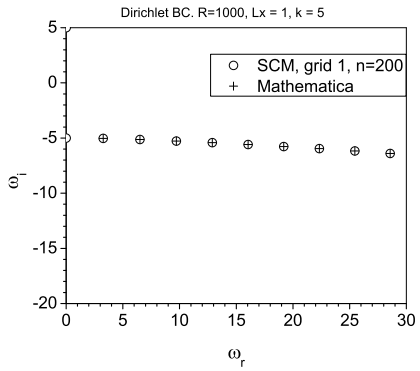

Figure 7. Comparison of eigenvalues obtained using SCM and Mathematica at $R = 1000$, $k = 5$, and $L_x = 1$.

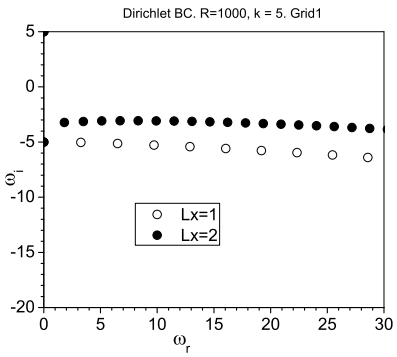

Figure 8. Comparison of eigenvalues at $L_x = 1$ and $L_x = 2$ obtained using SCM. $R = 1000$, $k = 5$.

Figure 11 shows comparison of the SCM result with result obtained using Mathematica. The comparison demonstrates that the splitting is associated with a loss of accuracy in the SCM data. Decreasing of number of polynomials n leads to loss of accuracy at lower ω_r as it is shown in Fig. 12.

Downloaded by Anatoli Tumin on August 27, 2019 | http://arc.aiaa.org | DOI: 10.2514/6.2011-3603

Downloaded by Anatoli Tumin on August 27, 2019 | http://arc.aiaa.org | DOI: 10.2514/6.2011-3603

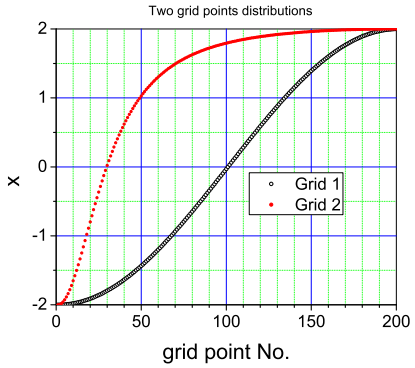

Figure 9. The grid points distribution at $x_i = 0.5$ (grid 1) and $x_i = 0.9$ (grid 2).

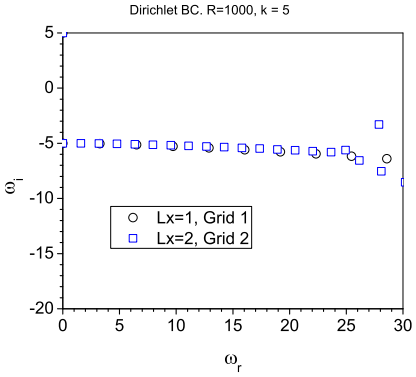

Figure 10. Comparison of SCM results obtained at $L_x = 1$ (grid 1) and $L_x = 2$. (grid 2).

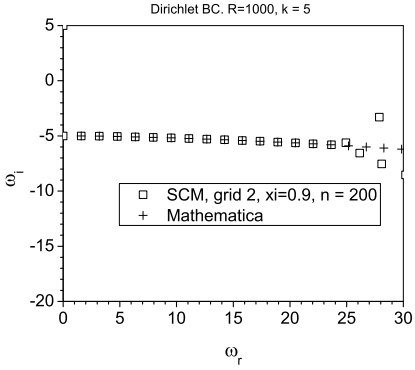

Figure 11. Comparison of SCM results with results obtained using Mathematica at $L_x = 2$, $x_i = 0.9$, $R = 1000$, $k = 5$, and $n = 200$.

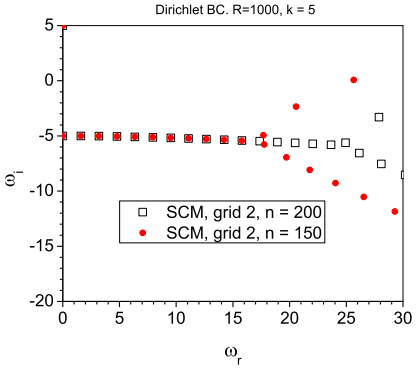

Figure 12. Comparison of SCM results obtained with $n = 200$ and $n = 150$ at $L_x = 2$, $x_i = 0.9$, $R = 1000$, and $k = 5$.

II.B. Box formulation with Fourier discretization in the vertical direction

In the case that the global modes are computed via the numerical solution of a two-dimensional PDEs problem within the "box formulation" with finite L_x and L_y, the linearized Navier-Stokes equations, after using the Laplace transform in time, can be written as

$$-i\omega \mathbf{H}_t \mathbf{A} = \mathbf{H}\mathbf{A}, \tag{7}$$

where the matrix $\mathbf{H}$ involves derivative operators in the two spatial directions. The numerical solution requires truncation and discretization of the domain. The $x-$direction is discretized using the same Chebyshev SCM as in the tall box formulation. A Fourier collocation method is used for the discretization of the $y-$direction, thus imposing periodicity in the domain length. N_x and N_y are the number of discretization points in x and y directions. The periodicity lengths are then determined by the domain truncation L_y; The different lengths $L_y = \pi/5, 2\pi/5, 4\pi/5$ and $10\pi/5$ were used in order to permit wavenumbers that are integer multiples of $k = 5/2$, suitable for comparison with figure 2.

Figure 13 shows the convergence history of the spectra corresponding to $R = 1000$ and $L_y = \pi/5$. The number of discretization points on the streamwise direction N_x was increased from 100 to 200, while $N_y = 71$ was kept constant. Increasing N_y does not produce realizable changes in the eigenvalues. For the lower resolution $N_x = 100$ (black crosses in the figure), vertical branches are apparent in the spectrum with the upper tip skewed to higher frequencies (to the right), in the same manner that has been observed in the literature, as pointed out in the previous section. As N_x is increased to 150 (blue pluses in figure 13), the branches move to higher damping rates, while the real frequencies remain nearly constant. An additional set of eigenvalues also appear, at different frequencies than the vertical branches. When $N_x = 200$ (red squares in the figure), the vertical branches have disappeared, showing that they were an artifact of a lack of resolution. On the other hand, the differentiated line of eigenvalues that appeared first for $N_x = 150$ is accurately recovered for $N_x = 200$ too. These eigenvalues correspond with the $k = 5$ modes that were obtained in the tall-box formulation. In addition, a second line of converged eigenvalues corresponding to $k = 10$ is clearly defined.

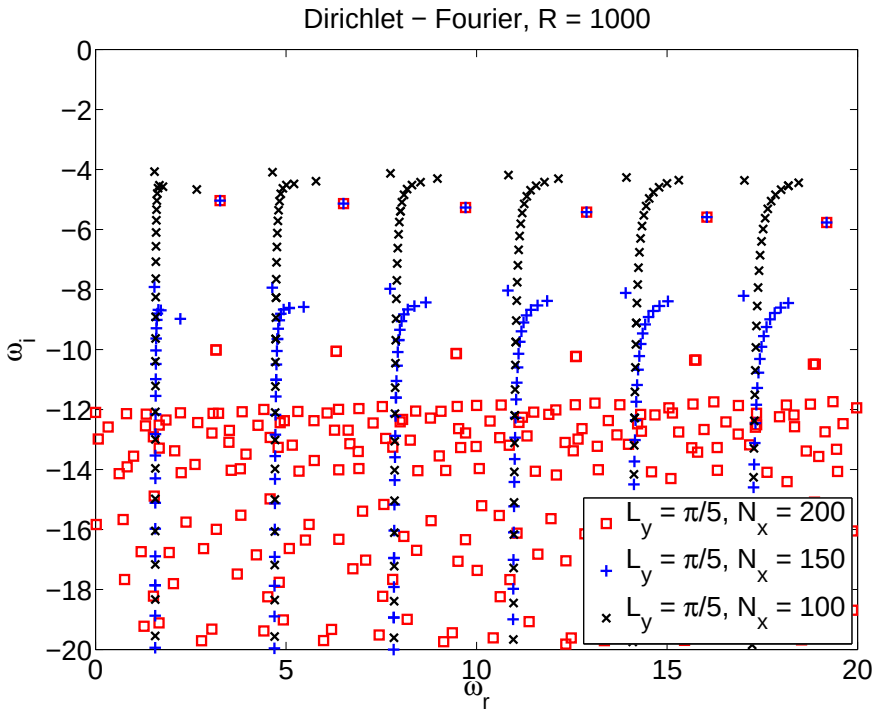

Figure 13. Spectrum at $R = 1000$ using the box formulation and different resolutions.

Figures 14 and 15 show the spectra corresponding to $R = 100$ and $R = 1000$ with different domain truncations L_y. The number of discretization points used are enough to ensure convergence of the eigenvalues

Downloaded by Anatoli Tumin on August 27, 2019 | http://arc.aiaa.org | DOI: 10.2514/6.2011-3603

forming the branches predicted by the tall-box formulation. By increasing L_y, additional eigenvalues are obtained in the different branches, corresponding to the intermediate values of k permitted.

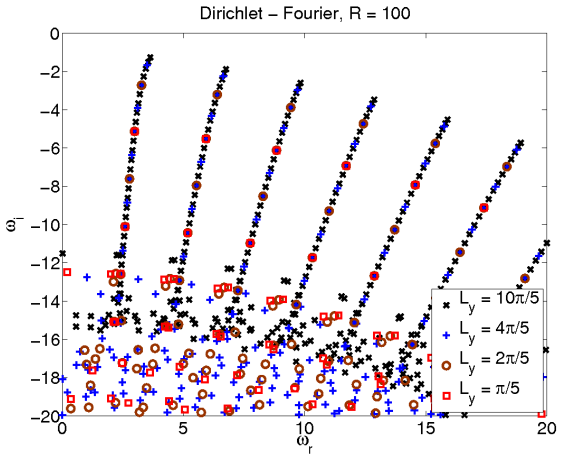

Figure 14. Spectrum at $R = 100$ using the box formulation

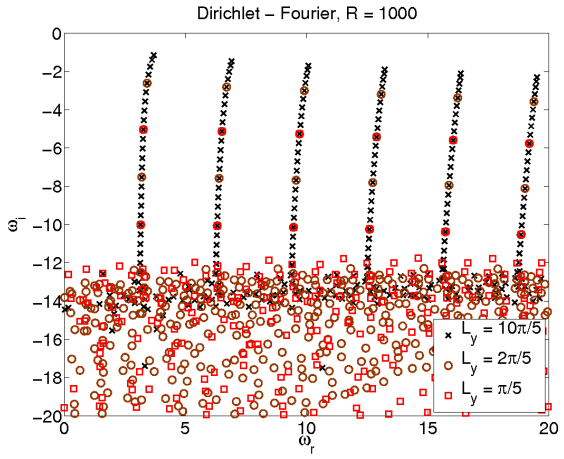

Figure 15. Spectrum at $R = 1000$ using the box formulation

Figures 16 and 17 show respectively the magnitudes of the streamwise and vertical velocity of modes 1 through 4 at $R = 1000$ and $k = 5$, obtained using the box formulation. The boundary layer at the vicinity of $x = 1$ is shown in higher detail in the figures at the right in perfect agreement with the results of the tall-box formulation. Figure 17,b remarks the prediction that the spatial extent of the boundary layer that appears on the vorticity modes on account of the boundary conditions at $L_x = 1$ is nearly independent of the wavenumber k for increasingly high Reynolds numbers.

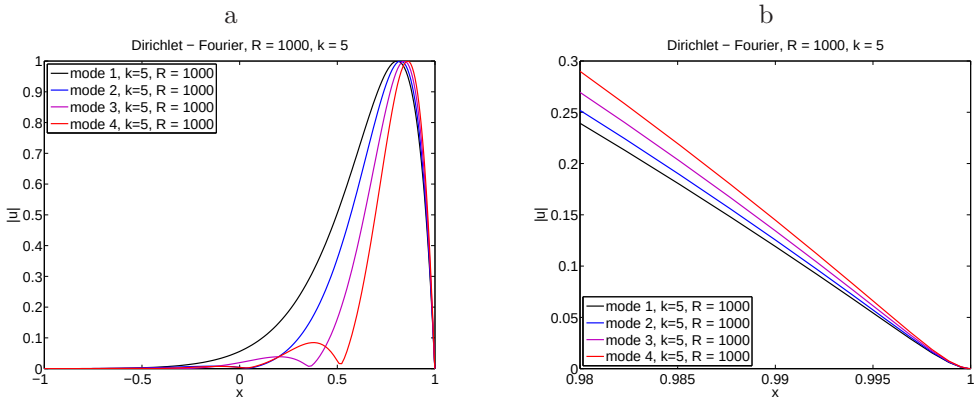

Figure 16. Streamwise velocity profiles in modes 1 through 4 at $R = 1000$ and $k = 5$.

II.C. Box formulation with Dirichlet boundary conditions

In the previous subsections, Dirichlet homogeneous boundary conditions were imposed only to the streamwise and vertical velocity components, at $x = \pm L_x$. Periodicity was imposed on the $y-$direction either directly in the tall-box formulation, or via Fourier collocation in the box-formulation. No additional boundary conditions were required for the pressure.

In this subsection the effect of using a bounded box, without periodic boundary conditions in the transversal direction is studied, and a Chebyshev discretization for the $y-$direction is introduced. In this case, the pressure variable needs some special treatment. Several possibilities have been proposed in the literature,[2,3] trying to minimize its impact on the visual aspect of the global eigenfunctions. In the spirit of the present model, the simplest homogeneous Dirichlet boundary conditions are applied also to the pressure variable at all boundaries. In order to make direct comparison with a Chebyshev-Fourier discretization, the computations of the previous subsection were repeated but imposing also the homogeneous Dirichlet boundary

Downloaded by Anatoli Tumin on August 27, 2019 | http://arc.aiaa.org | DOI: 10.2514/6.2011-3603

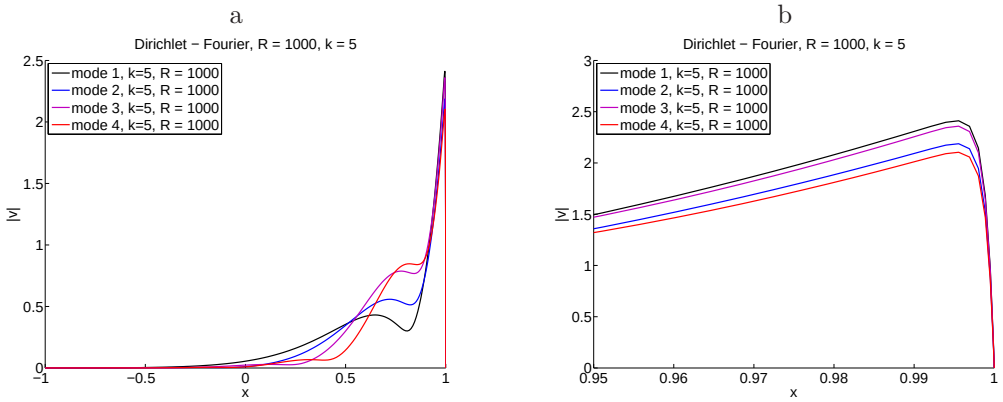

Figure 17. Vertical velocity profiles in modes 1 through 4 at $R = 1000$ and $k = 5$.

Downloaded by Anatoli Tumin on August 27, 2019 | http://arc.aiaa.org | DOI: 10.2514/6.2011-3603

condition to the pressure at $x = \pm L_x$:

$$u(x = \pm L_x, y) = v(x = \pm L_x, y) = p(x = \pm L_x, y) = 0. \tag{8}$$

The domain was truncated at $L_y = 5\pi$. When the Chebyshev discretization is used for the y-direction, homogeneous Dirichlet boundary conditions are also imposed to the upper and lower boundaries.

$$u(x, y = \pm L_y) = v(x, y = \pm L_y) = p(x, y = \pm L_y) = 0. \tag{9}$$

Figure 18 shows the spectra corresponding to the finite box, using a Fourier collocation method (crosses) and Chebyshev collocation method along with homogeneous Dirichlet boundary conditions (pluses). While there is not a one-to-one correspondence of the eigenvalues recovered with the two discretizations, they lump forming the same branches. As opposed to the cases presented in the previous section, where the branches described nearly straight lines, in the present spectra the branches are curved lines.

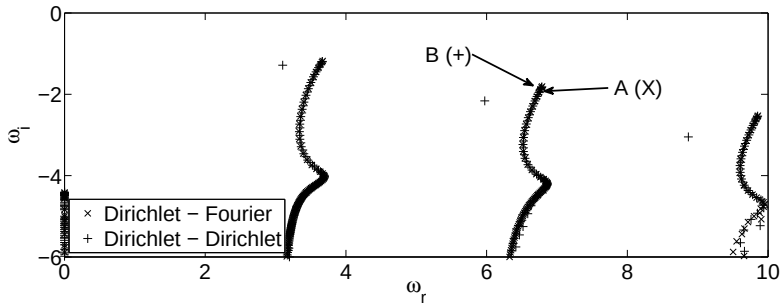

Figure 18. Spectra corresponding to the domain $[-1, 1] \times [-5\pi, 5\pi]$ at $Re = 100$. Crosses and pluses denote the eigenvalues corresponding to the Fourier and Chebyshev (with Dirichlet boundary conditions) discretization in the y-direction, respectively.

The different eigenvalues appearing in the branches can be denumerated according to their relative position on the branch. This order is related also to the number of peaks and valleys that can be identified in the eigenfunctions. Figures 19 to 22 illustrate streamwise velocity perturbations for the modes A and B, highlighted in Figure 18. Mode A is obtained using the Chebyshev-Fourier discretization, while mode B is obtained using a Chebyshev-Chebyshev discretization with Dirichlet boundary conditions. Figures 19 and 21 show the real component of the streamwise velocity for modes A and B, respectively. Except for the particular behavior imposed by the discretization in the vicinity of the $y = \pm L_y$, the main features are identical. The agreement is more remarked for figures 20 and 22, corresponding to the streamwise velocity magnitude at the $y = 0$ section.

The amplitude functions obtained for a bounded box in which homogeneous boundary conditions are imposed to all the boundaries are shown to be in good agreement with those for the tall-box formulation,

except for a new boundary layer existing in the vicinity of $y = \pm L_y$. As can be inferred from figure 21, this boundary layer may require large numbers of collocation points to be resolved, otherwise resulting into spurious oscillations of the amplitude functions.

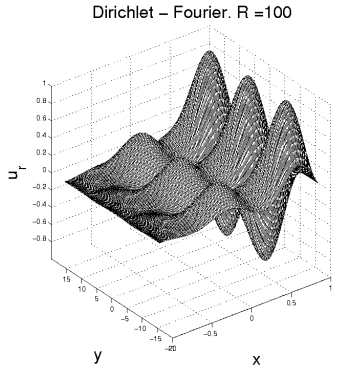

Figure 19. Streamwise velocity perturbation in mode A.

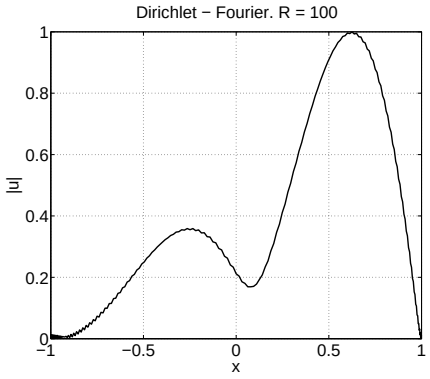

Figure 20. Profile of the maximum streamwise velocity perturbation in mode A.

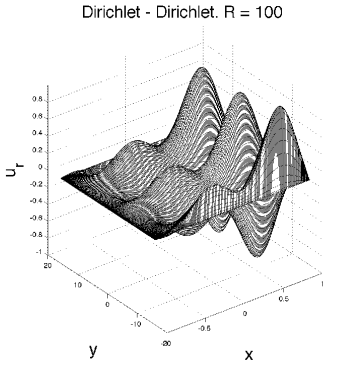

Figure 21. Streamwise velocity perturbation in mode B.

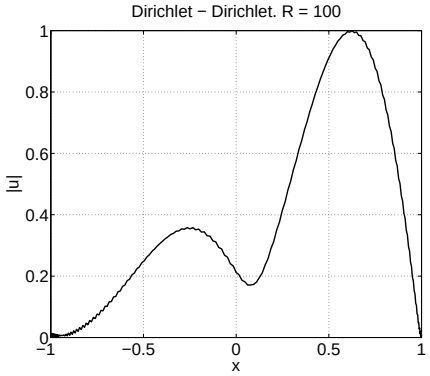

Figure 22. Profile of the maximum streamwise velocity perturbation in mode B.

Downloaded by Anatoli Tumin on August 27, 2019 | http://arc.aiaa.org | DOI: 10.2514/6.2011-3603

Downloaded by Anatoli Tumin on August 27, 2019 | http://arc.aiaa.org | DOI: 10.2514/6.2011-3603

III. Initial value problem using global modes

III.A. Analytical solution for the unbounded problem

The solution of a model initial value problem (IVP) by means of projecting the initial condition on the set of global eigenmodes for an unbounded flow is considered now. An exact analytical solution of the problem is obtained by using the Laplace transform in time and Fourier transforms for the spatial directions. After the transformations, the linear equations for each mode $\mathbf{A}_{\alpha k}$ result

$$(s\mathbf{H}_t + \mathrm{i}k\mathbf{I} - \mathbf{H}_1 - \mathrm{i}\alpha\mathbf{H}_2)\mathbf{A}_{\alpha k} = \mathbf{H}_t\mathbf{A}_{0,\alpha k}, \tag{10}$$

where s is the variable in the Laplace space[a], $\mathbf{I}$ is the identity matrix and $\mathbf{A}_{0,\alpha k}$ is the (α, k) component of the initial condition. The solution of (10) is obtained directly

$$\mathbf{A}_{\alpha k} = (s\mathbf{H}_t + \mathrm{i}k\mathbf{I} - \mathbf{H}_1 - \mathrm{i}\alpha\mathbf{H}_2)^{-1}\mathbf{H}_t\mathbf{A}_0 \tag{11}$$

Inverse Laplace transform is applied now, taking into account that the dispersion relation only contains the discrete pole $s^*_{\alpha k} = -\mathrm{i}\alpha - (\alpha^2 + k^2)/R$:

$$\begin{aligned} \mathbf{A}_{\alpha k}(t) &= \frac{1}{2\pi\mathrm{i}}\int_\Gamma \mathbf{A}_{\alpha k}(s)\ \mathrm{e}^{st}\ ds = \frac{1}{2\pi\mathrm{i}} Res(\mathbf{A}_{\alpha k}(s))|_{s=s^*}\ \mathrm{e}^{s^* t} \\ &= C_{\alpha k}\hat{\mathbf{A}}_{\alpha k}\ \mathrm{e}^{s^* t}. \end{aligned} \tag{12}$$

The coefficient $C_{\alpha k} = (-\alpha k A_{0,u} + \alpha^2 A_{0,v})/(\alpha^2 + k^2)$ is obtained from the projection of the initial condition on the mode $\hat{\mathbf{A}}_{\alpha k} = (-k/\alpha,\ 1,\ 0)^T$. Once the initial condition is projected on the modes, inverse Fourier transforms deliver the temporal evolution of the disturbance flow:

$$\mathbf{A}(x, y, t) = \frac{1}{4\pi^2}\int_0^\infty \int_0^\infty C_{\alpha k}\hat{\mathbf{A}}_{\alpha k}\mathrm{e}^{s^*_{\alpha k} t}\ e^{i\alpha x} e^{iky}\ d\alpha\ dk. \tag{13}$$

III.B. Solution using two-dimensional global modes

When the box formulation is considered and the global modes are obtained as the numerical solution of a two-dimensional eigenvalue problem on PDEs, an analogous development is introduced. Applying the Laplace transform in time, we have

$$(s\mathbf{H}_t - \mathbf{H})\mathbf{A} = \mathbf{H}_t\mathbf{A}_0. \tag{14}$$

The solution to this problem can be obtained using the variation of the parameters method. First a general solution for the homogeneous problem is sought, leading to the linear eigenvalue problem discussed in the previous sections. Note that the two-dimensional eigenvalue problem is solved numerically, and then only a finite number of discrete eigenmodes are recovered. The solution to the homogeneous problem is a linear combination of the different eigenmodes. The solution to the inhomogeneous problem can then be written as

$$\mathbf{A}_p(x, y, s) = \sum_j a_j(s)\hat{\mathbf{A}}_j(x, y). \tag{15}$$

Substituting (15) in (14):

$$\sum_j a_j(s)(s\mathbf{H}_t - \mathbf{H})\hat{\mathbf{A}}_j = \mathbf{H}_t\mathbf{A}_0. \tag{16}$$

However, at this point it is not possible to determine the functions $a_j(s)$. Because of the non-normal nature of the linearized Navier-Stokes equations, the eigenvectors $\hat{\mathbf{A}}_j$ do not form an orthogonal basis. A bi-orthogonality condition can be derived using the eigenvectors of an adequately defined adjoint problem.

[a] Note that the complex frequency ω, kept in the previous sections in line with classic linear stability theory, has been replaced by $s = -\mathrm{i}\omega$.

An inner product of two complex functions $\mathbf{a}$ and $\mathbf{b}$ defined in the space Ω is introduced as

$$< \mathbf{a}, \mathbf{b} >= \int_{\Omega} \mathbf{a}^{\dagger} \cdot \mathbf{b} \; d\Omega, \tag{17}$$

where the subscript † denotes complex conjugation. Applying this inner product to an arbitrary function $\tilde{\mathbf{A}}$ and to the homogeneous problem, and then using integration by parts to transpose the linear operators inside the inner product, we have

$$< \tilde{\mathbf{A}}, (s\mathbf{H}_t - \mathbf{H})\hat{\mathbf{A}} >= \mathbf{P}(\tilde{\mathbf{A}}, \hat{\mathbf{A}}) - < (s^{\dagger}\mathbf{H}_t - \mathbf{H}^{\dagger})\tilde{\mathbf{A}}, \hat{\mathbf{A}} > . \tag{18}$$

$\mathbf{P}(\tilde{\mathbf{A}}, \hat{\mathbf{A}})$ is the so-called bilinear concomitant, and only depends on the values $\tilde{\mathbf{A}}$ and $\hat{\mathbf{A}}$ at the domain boundaries. The second term at the right-hand-side of (18) defines the adjoint problem

$$(s^{\dagger}\mathbf{H}_t - \mathbf{H}^{\dagger})\tilde{\mathbf{A}} = 0. \tag{19}$$

The adjoint problem contains the same eigenvalues as the direct problem, while the eigenvectors are different. It can be shown that between the direct and adjoint eigenvectors hold the bi-orthogonality relation

$$0 = (s_j - s_l) < \tilde{\mathbf{A}}_l, \mathbf{H}_t\hat{\mathbf{A}}_l > . \tag{20}$$

For the derivation of the condition (20) it is necessary that the bilinear concomitant $\mathbf{P} = 0$. This condition constrains the set of boundary conditions that can be applied to the adjoint eigenvalue problem. Imposing Dirichlet homogeneous boundary conditions to all variables trivially satisfies this condition.

Projecting now equation (16) on the adjoint eigenvector $\tilde{\mathbf{A}}_j$, and taking into account (20):

$$< \tilde{A}_j, \sum_j a_j(s\mathbf{H}_t - \mathbf{H})\hat{\mathbf{A}}_j >=< \tilde{\mathbf{A}}_j, \mathbf{H}_t\mathbf{A}_0 > . \tag{21}$$

The previous expression can be solved for $a_j(s)$, and the solution to the inhomogeneous problem can then be written as

$$\mathbf{A}_p(x, y, s) = \sum_j \frac{< \tilde{\mathbf{A}}_j, \mathbf{H}_t\mathbf{A})0 >}{< \tilde{\mathbf{A}}_j, (s\mathbf{H}_t - \mathbf{H})\hat{\mathbf{A}}_j >} \; \hat{\mathbf{A}}_j(x, y). \tag{22}$$

Applying now the inverse Laplace transform:

$$\mathbf{A}(x, y, t) = \frac{1}{2\pi \mathrm{i}} \int_{\Gamma} \mathbf{A}_p(x, y, s)\mathrm{e}^{st} ds = \frac{1}{2\pi \mathrm{i}} \sum_j Res(\mathbf{A}_p)|_{s=s_j} \; \mathrm{e}^{s_j t}. \tag{23}$$

It can be shown that the residual of $\mathbf{A}_p$ at the pole s_j is

$$Res(\mathbf{A}_p)|_{s=s_j} = 2\pi \mathrm{i} \frac{< \tilde{\mathbf{A}}_j, \mathbf{H}_t\mathbf{A}_0 >}{< \tilde{\mathbf{A}}_j, \mathbf{H}_t\hat{\mathbf{A}}_j >}. \tag{24}$$

Now we can define the initial modal amplitudes as $C_j =< \tilde{\mathbf{A}}_j, \mathbf{H}_t\mathbf{A}_0 > / < \tilde{\mathbf{A}}_j, \mathbf{H}_t\hat{\mathbf{A}}_j >$, and write the solution to the initial value problem as

$$\mathbf{A}(x, y, t) = \sum_j C_j \hat{\mathbf{A}}_j(x, y) \; \mathrm{e}^{s_j t}. \tag{25}$$

III.C. Results

A model vortex is used as initial condition, defined by the distribution of rotational velocity $V_{rot} = a \cdot r \; \exp[-(r/b)^2]$. Here r is the radial coordinate measured from the center of the vortex, and the parameters a and b are determined in order to have a maximum velocity equal to one and a fast decay in the velocity distribution (at $r = 1$ the velocity magnitude is $O(10^{-10})$). At the initial instant the center of the vortex is located at $(x, y) = (1, 0)$. The spatial structure of this model vortex is the same that was used to model the actuator in some theoretical active flow control studies based on projection on the global eigenmodes.[7,8] Figures (23-24) show the temporal evolution of the model vortex computed as the superposition of global

Downloaded by Anatoli Tumin on August 27, 2019 | http://arc.aiaa.org | DOI: 10.2514/6.2011-3603

eigenmodes on the box-formulation, and compared to the exact analytical solution for an unbounded domain. Note that the fields corresponding to $t = 0$ are the initial projection of the model vortex on the subset of eigenmodes.

Two different boxes are used: $[0, 4] \times [-1, 1]$ and $[0, 8] \times [-1, 1]$. Following the previous section, homogeneous Dirichlet boundary conditions are imposed at all boundaries for the velocity components and pressure. Despite the deviation from the "tall box" problem (L_y is not large now), the qualitative description of the amplitude functions remains identical with those modes discussed above (figures 21-22).

The projection of the initial condition on a finite number of eigenmodes inherits the large amplitude oscillations in the vicinity of the outlet that characterizes the amplitude functions of the individual eigenmodes. Figure 23 shows the vortex evolution projected on the 250 eigenmodes closer to $\omega = 0$. The unphysical structure seen is not limited to a narrow boundary layer, but extends to the entire domain for $t = 0$, overwhelming the amplitude of the model vortex. With increasing time, this structure seems to be convected downstream while it decays in amplitude. If we consider the evolution of the projected disturbance field given at $t = 0$, we can conclude that it is reasonable on physical grounds; it is the projection of the initial condition on the finite set of eigenmodes that introduces the oscillations. Increasing the domain length in the streamwise direction is not helpful in reducing the oscillations. In fact, doubling the domain length introduces new eigenmodes, the amplitude functions of which present longer wavelengths. A larger number of eigenmodes would then be required in order to resolve the initial vortex model with the same degree of detail. This manifests itself in figure 23, where the vortex projected on the $[0, 8] \times [-1, 1]$ box is stretched in the streamwise direction. Figure 24 shows the vortex evolution projected on the first 750 eigenmodes. The unphysical oscillations are reduced both in amplitude and in extent for the initial projection, and are reduced faster as t is increased.

The emergence of unphysical structures in the bi-orthogonal projection of the model vortex was also found in Refs.,[7,8] but they attributed it to numerical inaccuracies in the computation of the projection coefficients C_j (in equation 25), due to the spatial separation between the direct and adjoint eigenfunctions. The present results show that the unphysical structure actually diminishes when a larger number of modes is used in the projection, indicating that it could be eliminated if a very large, probably impractical, number of modes were used.

IV. Summary and conclusions

A simple model problem has been considered in order to understand the effect of upstream and downstream boundary conditions on the eigenvalues and eigenfunctions delivered by the solution of global stability eigenvalue problems. The possible limitations of the global mode formulation and its application to the solution of initial value problems have been discussed. The eigenmode expansion of the perturbations on a 2D uniform flow is addressed using three formulations: (a) an exact analytical formulation considering unbounded flow, (b) a "tall-box" formulation for which the domain is bounded on the streamwise direction but not in the transversal direction, and (c) a "box-formulation" in which the domain is bounded on both directions, which corresponds to the usual global stability problem.

It is shown that applying the box-formulation to an unbounded flow introduces artifacts such as upstream pressure and vorticity waves. The pressure wave penetrates upstream in the domain at a distance of approximately the characteristic scale of the perturbation in the y direction. In addition, the upstream vorticity wave introduces a boundary layer of extent $O(1/R)$ within the downstream boundary of the domain, giving rise to strong gradients in the eigenfunctions. In order to have the physical picture unaffected by the boundary conditions, the size of the box should be chosen depending on the typical scales of the perturbations under consideration. On the other hand, the artificial boundary layers also appear in the vicinity of the upper and lower boundaries in the box-formulation. Large resolutions in both spatial directions might be necessary in order to resolve this boundary layers; otherwise shifts in the eigenspectrum appear, as well as pointwise oscillations in the eigenfunctions that prevent them from being used in a normal mode projection. The combined need for a large box and high resolution in two spatial directions results in the large memory requirements associated with the solution of the global eigenvalue problem.

Uniform flow cannot sustain growth of perturbations, due to the absence of a shear component. Consequently, the spatial growth of the velocity perturbations observed in the global modes is not related to a spatial amplification associated with convective instability, but is an artifact of the box-formulation. This result should serve as a warning in interpreting analogous observations in recent global instability analyses.

Downloaded by Anatoli Tumin on August 27, 2019 | http://arc.aiaa.org | DOI: 10.2514/6.2011-3603

Downloaded by Anatoli Tumin on August 27, 2019 | http://arc.aiaa.org | DOI: 10.2514/6.2011-3603

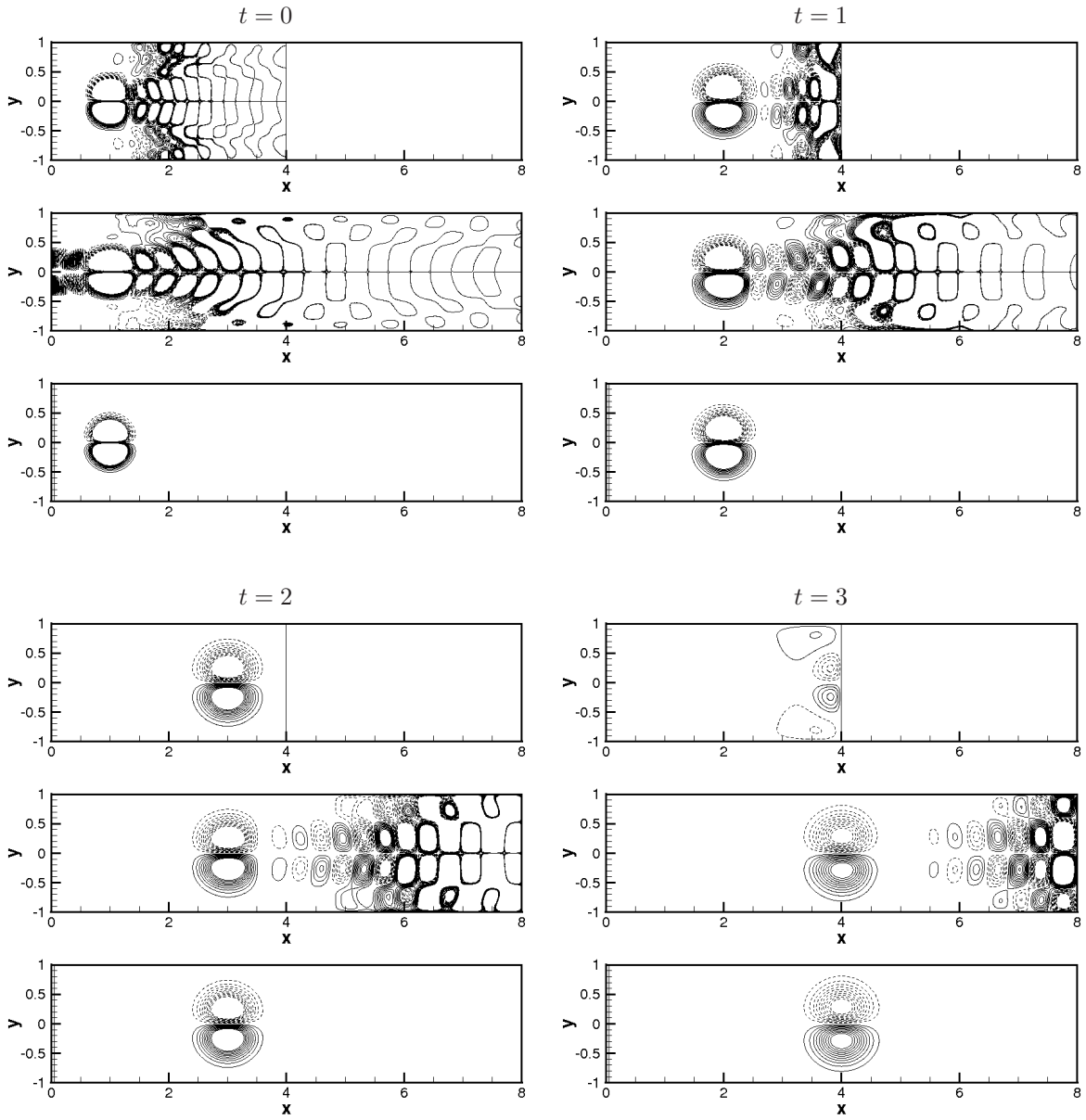

Figure 23. Evolution of the model vortex. For each time t instant and set of boundary conditions, upper and intermediate plots correspond to the projection on global modes computed on the domains $[0, 4] \times [-1, 1]$ and $[0, 8] \times [-1, 1]$, respectively. Lower plots correspond to the analytical solution for unbounded flow. The initial condition was projected on the leading 250 global modes. The lower plot corresponds to the analytic solution. Contour lines correspond to streamwise velocity $\hat{u}$ with a constant spacing of 0.1. Negative $\hat{u}$ values are denoted by dashed lines.

Downloaded by Anatoli Tumin on August 27, 2019 | http://arc.aiaa.org | DOI: 10.2514/6.2011-3603

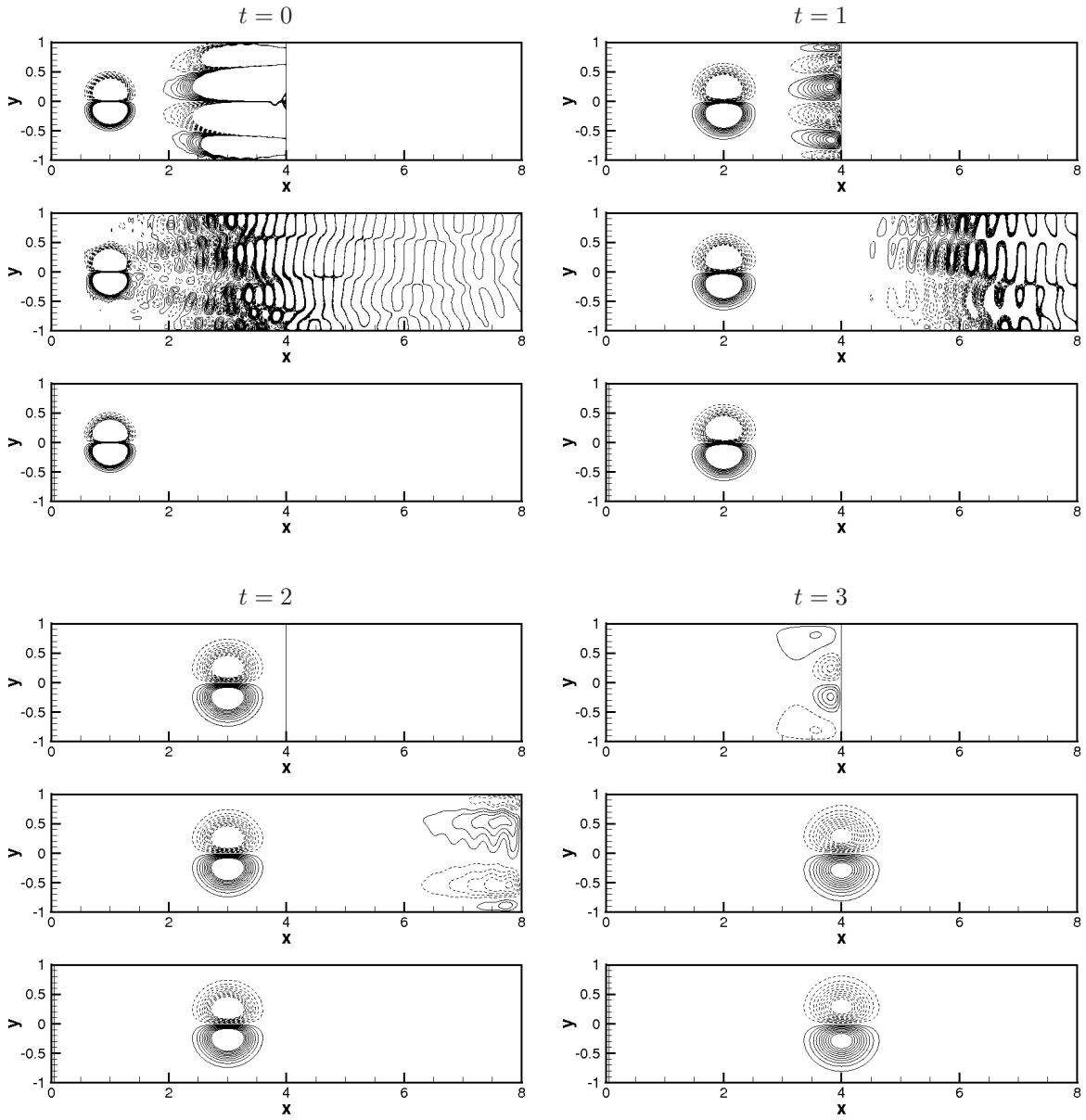

Figure 24. Evolution of the model vortex. For each time t instant and set of boundary conditions, upper and intermediate plots correspond to the projection on global modes computed on the domains $[0, 4] \times [-1, 1]$ and $[0, 8] \times [-1, 1]$, respectively. Lower plots correspond to the analytical solution for unbounded flow. The initial condition was projected on the leading 750 global modes. The lower plot corresponds to the analytic solution. Contour lines correspond to streamwise velocity $\hat{u}$ with a constant spacing of 0.1. Negative $\hat{u}$ values are denoted by dashed lines.

Furthermore, the spatial structure of the global modes can make the solution of initial value problems via normal mode projection extremely challenging. The temporal evolution of a model vortex on the uniform flow was considered in order to illustrate this possibility. The vortex, located initially near the upstream boundary, is projected using the bi-orthogonal relation between its direct and adjoint modes. In the normal mode expansion, unphysical structures emanating from the downstream boundary are present alongside the known vortex. These unphysical structures arise from the particular shape of the global modes recovered in the box formulation. An unaffordably large number of modes needs to be introduced into the projection in order to reduce the amplitude of the numerical artifacts so that the evolution of the initial condition can be reliably computed, without interference from unphysical structures introduced by the artificial boundary closure.

It should be noted that the results presented herein are only representative of a particular choice of boundary conditions, while they share many of the characteristics found in global instability analysis of open flows in the literature. Assuming that the two-dimensional eigenvalue problem leads to a complete set of eigenfunctions, the discussion on the correctness of the boundary conditions in the box formulation is not sensible. The discussion should address the appropriateness of the set of eigenfunctions for the specific problem.

Downloaded by Anatoli Tumin on August 27, 2019 | http://arc.aiaa.org | DOI: 10.2514/6.2011-3603

Acknowledgments

D.R. acknowledges the sponsorship by the AFOSR Grant No FA8655-06-1-3066 to *nu modelling s.l.*, entitled *Global instabilities in laminar separation bubbles*. The Grant is monitored by Dr. D. Smith of AFOSR (originally by Lt. Col. Dr. Rhett Jefferies) and Dr. S. Surampudi of EOARD. D.R. also acknowledges partial funding by the Marie Curie-UPM-COFUND UNITE programme.

A.T. was sponsored by the AFOSR/NASA National Center for Hypersonic Research in Laminar-Turbulent Transition and by the Air Force Office of Scientific Research, USAF, under Grant No. FA9550-08-1-0322 monitored by Dr. J. D. Schmisseur. The views and conclusions contained herein are those of the author and should not be interpreted as necessarily representing the official polices or endorsements, either expressed or implied, of the Air Force Office of Scientific Research or the U. S. Government.

V.T. acknowledges the funding by the MICINN, under Grant No. TRA2009-13648, entitled "Metodologías computacionales para la predicción de inestabilidaes globales hidrodiámicas y aeroacústicas de flujos complejos".

Computations have been performed on the Centro de Supercomputación de Galicia (CESGA) facilities.

References

[1]Theofilis, V., "Advances in global linear instability of nonparallel and three-dimensional flows," *Prog. Aero. Sciences*, Vol. 39 (4), 2003, pp. 249–315.

[2]Ehrenstein, U. and Gallaire, F., "On two-dimensional temporal modes in spatially evolving open flows: the flat-plate boundary-layer," *J. Fluid Mech.*, Vol. 536, 2005, pp. 209–218.

[3]Åkervik, E., Ehrenstein, U., Gallaire, F., and Henningson, D. S., "Global two-dimensional stability measures of the flat plate boundary-layer flow," *European J. Mech. B/Fluids*, Vol. 27, 2008, pp. 501–513.

[4]Rodríguez, D. and Theofilis, V., "On instability and structural sensitivity of incompressible laminar separation bubbles in a flat-plate boundary layer," *AIAA Paper 2008-4148*, 2008.

[5]Bagheri, S., Åkervik, E., Brandt, L., and Hennigson, D. S., "Matrix-free methods for stability and control of boundary layers," *AIAA J.*, Vol. 57, 2009, pp. 1057–1068.

[6]Bagheri, S., Hennigson, D. S., Hœpffner, J., and Schmid, P. J., "Input-output analysis and control design applied to a linear model of spatially developing flows," *Appl. Mech. Reviews*, Vol. 62, 2009, pp. 020803–1–020803–27.

[7]Alizard, F. and Robinet, J.-C., "Modeling of optimal perturbations in flat plate boundary layer using gloabl modes: benefits and limits," *Theor. Comp. Fluid Dyn.*, Vol. 25, 2011, pp. 147–165.

[8]Ehrenstein, U., Passaggia, P.-Y., and Gallaire, F., "Control of a separated boundary layer: reduced-order modeling using global modes revisited," *Theor. Comp. Fluid Dyn.*, Vol. 25, 2011, pp. 195–207.

[9]Theofilis, V., "Global linear Instability," *Ann. Rev. Fluid Mech.*, Vol. 43, 2011, pp. 19–53.

[10]Giannetti, F. and Luchini, P., "Structural sensitivity of the first instability of the cylinder wake," *J. Fluid Mech.*, Vol. 581, 2007, pp. 167–197.

[11]Tumin, A., "Multimode decomposition of spatially growing perturbations in a two-dimensional boundary layer," *Phys. Fluids*, Vol. 15, 2003, pp. 2525–2540.

Downloaded by Anatoli Tumin on August 27, 2019 | http://arc.aiaa.org | DOI: 10.2514/6.2011-3603

View publication stats